ChemComm

Multiple Selectivity-Determining Mechanisms of H2O2 Formation in Iron Porphyrin-Catalysed Oxygen Reduction

Journal:	*ChemComm*
Manuscript ID	CC-COM-10-2020-006701.R2
Article Type:	Communication

COMMUNICATION

Multiple Selectivity-Determining Mechanisms of H_2O_2 Formation in Iron Porphyrin-Catalysed Oxygen Reduction

Received 00th January 20xx,
Accepted 00th January 20xx

DOI: 10.1039/x0xx00000x

Anna C. Brezny,[†,a,b] Hannah S. Nedzbala[†,a] and James M. Mayer*[,a]

Multiple H_2O_2-forming mechanisms are accessible in Fe(porphyrin)-catalyzed oxygen reduction, a key reaction in both fuel cell technologies and oxygen-utilizing enzymes. Our kinetic analysis reveals that the porphyrin secondary structure dictates the pathway for H_2O_2 formation. This approach is generalizable to other electrocatalytic processes to gain insight into the selectivity-determining steps.

The ability to understand and tune the selectivity of electrocatalysts for the reduction of oxygen is valuable in many contexts. In the oxygen reduction reaction (ORR) in fuel cells, for example, it is important to have complete reduction of O_2 to H_2O rather than forming H_2O_2, which is corrosive and a less exoergic product.[1] Similar issues arise in biological oxygen reduction. More specifically, enzymes in the cytochrome P450 superfamily oxidize substrates via the complete, $4e^-$ reduction of O_2, but also produce significant H_2O_2.[2] This selectivity is believed to be controlled by groups in the active site pocket away from the iron centre. These groups appear to direct protonation of the Fe^{III}–OOH intermediate to either the proximal oxygen, producing H_2O_2, or the distal O which leads to H_2O (Figure 1, blue, black).[3,4,5] Iron porphyrin complexes are structurally similar to the heme active site in P450s, and have received considerable attention as molecular catalysts for the ORR and other reactions.[6-9]

Several reports using molecular ORR catalysts have demonstrated that changes to catalyst parameters such as overpotential[10,11] and second coordination sphere H-bonding groups[8,12-20] can have a marked effect on ORR selectivity. These studies suggest that the change in selectivity is due to the activation of the distal oxygen of the Fe^{III}–OOH intermediate towards

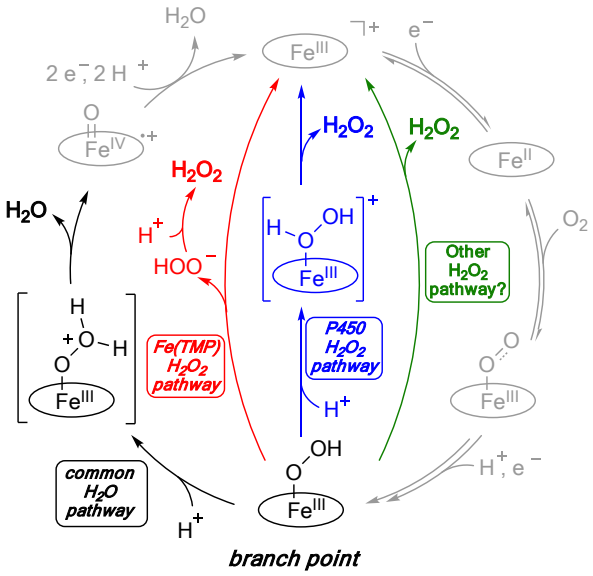

Figure 1. Mechanism of the ORR with Fe(P) catalyst highlighting the selectivity-determining steps, which occur after the rate-determining steps.[21,22]

protonation, which effectively increases the relative rate of H_2O formation over H_2O_2. These observations are in line with the cytochrome P450 mechanism where mutagenesis studies have demonstrated the importance of H-bonding networks to control selectivity.[3,4,5] Here we report that structural modifications to the porphyrin of Fe(P) electrocatalysts do not just change the relative formation of H_2O vs H_2O_2, they can also change the *mechanism* of H_2O_2 formation.

Study of the mechanistic step that defines selectivity in the ORR is challenging as it generally occurs after the rate-determining step.[7,21-23] This renders the selectivity-determining step kinetically invisible, and usually prevents the selectivity-relevant intermediates from being observed under catalytic conditions. Recently, we reported an analysis of H_2O_2 formation by iron(tetramesitylporphyrin) (Fe(TMP), **1**) in DMF, which implicated HOO^- dissociation from an intermediate Fe^{III}–OOH species instead of proximal protonation to form H_2O_2

[a] *Department of Chemistry, Yale University, New Haven, CT 06520, USA.*
[b] *Department of Chemistry, Skidmore College, Saratoga Springs, NY 12866, USA.*
† These authors contributed equally
Electronic Supplementary Information (ESI) available: [details of any supplementary information available should be included here]. See DOI: 10.1039/x0xx00000x

(Figure 1, red vs. blue paths).[21] The HOO^- species was then proposed to undergo rapid protonation to form H_2O_2. In this report, we investigate the selectivity-determining steps of a range of Fe(porphyrin) (Fe(P)) catalysts (Chart 1) to probe the possibility of accessing both this dissociative pathway (Figure 1 red) and the P450-like proximal protonation (Figure 1 blue). The porphyrin ligands (P) used have a range of steric bulk and possible hydrogen-bonding abilities in the second-coordination sphere, while their iron complexes all have similar $E_{1/2}(Fe^{III/II})$ values (within 100 mV, Chart 1).

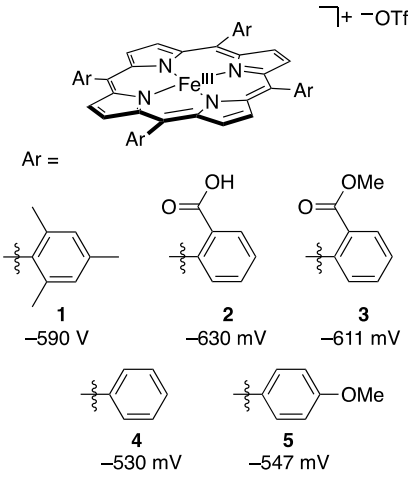

Chart 1. [Fe(P)][OTf] (OTf = trifluoromethanesulfonate) catalysts investigated in this study and their respective $E_{1/2}$ values of the Fe^{III}/Fe^{II} couple versus $Fc^{+/0}$.

The selectivity of the ORR was determined using rotating ring-disk voltammetry (RRDV).[7,12] Typical RRDV conditions employed 0.2 mM of iron catalyst ([Fe(P)][OTf], generated *in situ* from Fe(P)Cl and TlOTf), 100 mM $[NBu_4][PF_6]$, 1 atm (3.1 mM) O_2, and a range of acid concentrations from 10−200 mM [H-DMF][OTf] ([H-DMF]) in *N,N*-dimethylformamide (DMF).[23,24] RRDV is a classic technique to measure $\%H_2O_2$, in which the central disk is swept through reducing potentials to achieve catalysis while the outer ring is held at sufficiently high potentials to oxidize generated H_2O_2.[7,12] The ratio of these currents enables calculation of the $\%H_2O_2$.[23]

Kinetic experiments showed that all five Fe(P) display a rate law first order in [Fe(P)], [O_2], and [acid].[23] These results indicate a mechanism of O_2 binding to Fe^{II}(P) followed by rate-determining protonation to generate $[Fe^{III}(OOH^{\bullet})]^+$.[22] Consistent with our previous DFT calculations,[21] this protonated superoxo intermediate is likely rapidly reduced to the hydroperoxo complex, Fe^{III}–OOH.

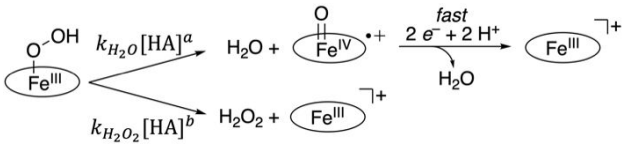

$$\log\left(\frac{[H_2O_2]}{[H_2O]}\right) = (b-a)\log([HA]) \qquad (1)$$

Scheme 1. Kinetic model for the red and blue ORR selectivity-determining steps from the Fe^{III}–OOH intermediate (see Figure 1).

Table 1. $\%H_2O_2$ values measured with **1** - **5** at a range of acid concentrations.

[H-DMF] (mM)	$\%H_2O_2$				
	1[a]	**2**	**3**	**4**	**5**
10	17 ± 2	5 ± 1	9 ± 1	-	10 ± 2
20	8.1 ± 0.7	6 ± 1	10 ± 3	14 ± 2	7.6 ± 2
30	-	-	-	12 ± 2	6.5 ± 0.9
50	3.2 ± 0.5	5 ± 1	9 ± 2	10 ± 2	5.2 ± 0.9
75	3.1 ± 0.2	5 ± 1	9 ± 2	-	5.4 ± 0.8
100	2.1 ± 0.5	5 ± 1	9 ± 1	9 ± 3	5.2 ± 0.6
200	-	-	-	8 ± 3	-

[a] Data from reference 21.

The basic kinetic model for catalytic selectivity involves two generic pathways from the putative Fe^{III}–OOH to H_2O or H_2O_2 (Scheme 1). The ferric-hydroperoxide is the species implicated as the selectivity bifurcation point in both molecular and enzymatic oxygen reduction by iron porphyrins.[2-9] To our knowledge, this species has not been directly observed as an intermediate in a functioning catalytic reaction, presumably because it is formed after the rate determining step and is present only in low concentrations. As noted above, Fe^{III}–OOH is a likely intermediate in these systems based on the kinetic and computational evidence for the protonated superoxide Fe^{III}–$OOH^{\bullet}$ being the product of the catalytic rate-determining step.

The selectivity-determining steps starting from Fe^{III}–OOH can have different kinetic orders in the concentration of acid, $[HA]^a$ or $[HA]^b$, as shown in Scheme 1 and as the red and blue paths in Figure 1 above. Equation 1 in Scheme 1, derived from rate laws based on this kinetic model,[21] predicts that plotting $\log([H_2O_2]/[H_2O])$ versus $\log([HA])$ should produce a line whose slope is $b–a$. This slope corresponds to the *difference in kinetic orders in [HA]* for the competing H_2O- and H_2O_2-forming pathways ($b–a$, eq 1).[23] For Fe(TMP) (**1**), we previously reported that increasing [HA] reduced the amount of H_2O_2 produced such that $b–a = –1$, indicating that the pathway for forming H_2O_2 has a kinetic dependence on [HA] that is one order lower than the H_2O pathway (Figure 1, red).[21] In this study, we performed the same analysis for the ORR catalysed by a variety of Fe(P) catalysts, **2–5**, recording $\%H_2O_2$ as a function of the concentration of [H-DMF] (Table 1). Interestingly, we observed a variety of the trends in $\%H_2O_2$ as a function of acid concentration.

In contrast with the trend observed for **1** ($b–a = –1$), the RRDV data for catalysts **2** and **3**, with possible hydrogen-bonding in the second coordination sphere, show that the H_2O_2 selectivity is

essentially independent of acid concentration (Figure 2A, dark blue and light blue data). The observation that $b–a \cong 0$ implies that catalysts **2** and **3** have a different pathway to H_2O_2, with different kinetic orders in acid, than was found for **1** ($b–a = –1$). With **1**, Fe^{III}-OOH is proposed to undergo initial HOO^- dissociation instead of protonation to form H_2O_2 (Figure 1, red).[21] The catalytic cycles for **2** and **3**, however, require protonation of Fe^{III}-OOH to release either H_2O or H_2O_2, thus mirroring the biological mechanism (Figure 1, blue and black).

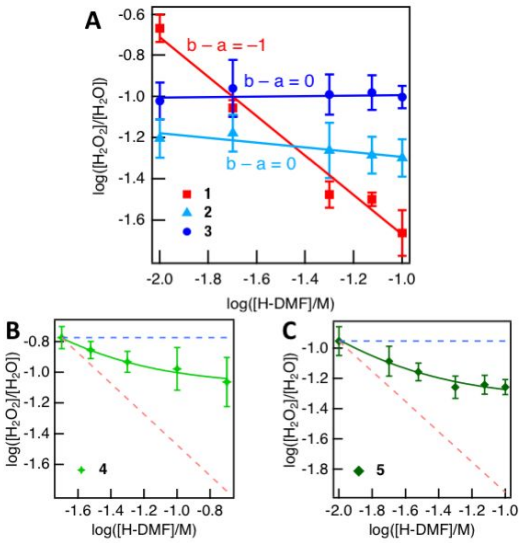

Figure 2. Plots of $\log([H_2O_2]/[H_2O])$ versus log([H-DMF]/M) for catalysts (**A**) **1**-**3**, (**B**) **4**, and (**C**) **5**. The slopes of the lines are representative of the difference in kinetic orders in acid for the H_2O_2- and H_2O-forming pathways (b–a). **A**: Solid lines are linear regression best fits of the data. **B** and **C**: Solid curved lines are fits from the kinetic model described in the ESI. The dashed lines are included just to guide the eye, showing the predicted behaviour for the paths to H_2O_2 in Figure 1: blue (labelled P450), b – a = 0 and red (labelled TMP), b – a = –1. The predicted lines are similar to the blue and red experimental data in part **A**.

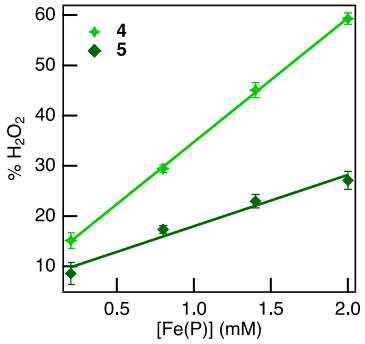

Figure 3. $\%H_2O_2$ versus catalyst concentration for catalysts **4** and **5**. Data were collected under typical conditions at the lowest acid concentration (20mM and 10mM [H-DMF][OTf] for **4** and **5**, respectively). Solid lines are linear regression best fits of the data.

Like the active sites in P450s, **2** and **3** have H-bonding groups in the second coordination sphere. We initially hypothesized that these H-bonding groups could cause the selectivity-determining mechanism to change from that observed with **1** to one that more closely resembles the biological mechanism. To investigate this, the same studies were carried out with catalysts **4** and **5**, both of which lack H-bonding groups in the *ortho* positions. Interestingly, the data for catalysts **4** and **5** imply a more complicated mechanistic picture. Results with both catalysts show a decreased production of H_2O_2 with increasing acid concentration, consistent with the trend observed for **1**, but with a non-linear relationship between $\log(H_2O_2/H_2O)$ and log([H-DMF]/M), with $–1 < b–a < 0$ (Figure 2B and C).

The non-integer slopes observed for catalysts **4** and **5** prompted further investigation into the selectivity-determining steps for catalysts **4** and **5.** Experiments conducted at a range of catalyst concentrations (0.2mM – 2.0mM) showed ORR selectivities that varied with the [Fe(P)] (Figure 3). This indicates that there is an H_2O_2-forming pathway for these catalysts that has a higher order in catalyst than the H_2O-forming pathway. In contrast, **1–3** show minimal dependence on catalyst concentration ($\Delta\ \%H_2O_2 < 8\%$ over an order of magnitude in [Fe(P)]), indicating that there are only small contributions from bimetallic pathways for these Fe(P) catalysts (see ESI Section 2.4 and Figures S12 and S15).[21]

Taken together, the different and curved reaction order plots (Figure 2) and the dependence on catalyst concentration (Figure 3) show that there are at least three competing H_2O_2-forming mechanisms (Scheme 2). For each catalyst, the changes in $\%H_2O_2$ as

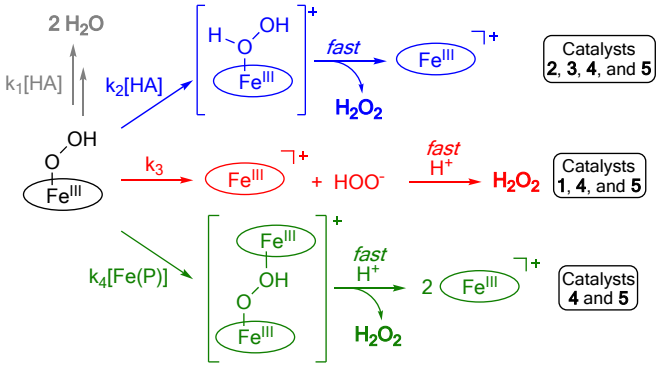

Scheme 2. Tentative mechanisms of H_2O_2 formation from the Fe^{III}–OOH intermediate. The proposed P450 mechanism (blue), TMP mechanism (red), and the bimetallic mechanism (green).

a function of [HA] or [Fe(P)] indicates that the H_2O and H_2O_2 pathways have different orders in that reactant. Based on the above trends in selectivity as a function of [HA] and [Fe(P)], and under the assumption that the H_2O pathway is first order in acid and catalyst, the following mechanistic insights can be made:[21]

(i) Catalyst **1** shows a selectivity dependence on [HA] but not [Fe(P)], which implies that its H_2O_2 pathway is zero order in [HA] and first order in [Fe(P)] (Scheme 2, red).[21]

(ii) Catalysts **2** and **3** display no selectivity dependence on [HA] and minimal selectivity dependence on [Fe(P)], which indicates that the primary H_2O_2 pathway is first order in both [HA] and [Fe(P)] for both catalysts under the reported conditions (Scheme 2,

blue). This is the same mechanism as is proposed for P450s, and thus it is possible that H-bonding is involved in facilitating this behaviour.

(iii) Catalysts **4** and **5** exhibit some selectivity dependence on both [HA] and [Fe(P)], indicating that these catalysts likely follow more than one competing H_2O_2 pathway, including one that is second order in [Fe(P)] (Scheme 2, green). The lack of steric bulk in the active site of **4** and **5** could enable the formation of an Fe-O-O-Fe intermediate.[25]

We emphasize that this bimetallic step must occur *after* the turnover-determining step. The kinetics of catalytic turnover being first order in [Fe(P)], [O_2] and [DMF-H^+], the independent measurement of pre-equilibria, and DFT calculations all indicate that the rate limiting step is protonation of the iron superoxide complex.[22]

An initial kinetic model was developed for catalysts **2** - **5**, based on the proposed mechanisms in Scheme 2 (ESI Section 2.4). The curved lines in Figure 2B,C and ESI Figures S1 – S4 show that this model can closely fit the experimental data. This provides support for the mechanism in Scheme 2. Interestingly, this series of compounds shows no clear trend in either the H_2O_2 selectivity or the preferred H_2O_2-forming pathway as a function of catalyst $E_{1/2}$ or ORR overpotential (ESI Section 5). The lack of a trend contrasts with reports on other systems.[10] Further investigations into these proposed mechanisms are continuing.

The results reported here show the complexity of selectivity-determining parts of mechanism of the ORR catalysed by soluble iron porphyrin complexes. Trends in selectivity as a function of [HA] and [Fe(P)] provide kinetic information about mechanistic steps that occur after the rate-limiting step and are therefore invisible in many catalytic studies. Small changes to the structure of the catalyst in the second coordination sphere not only change the selectivity but also direct reactivity preferentially to one H_2O_2-forming path over another. The understanding derived from this analysis of the selectivity-determining steps will facilitate the design of improved catalysts for the ORR and other electrocatalytic processes.

This research was supported as part of the Center for Molecular Electrocatalysis, an Energy Frontier Research Center funded by the U.S. Department of Energy, Office of Science, Office of Basic Energy Sciences. A.C.B. was supported in part by both Skidmore College and a postdoctoral fellowship from the NIH (F32GM129890).

Conflicts of interest

There are no conflicts to declare.

Notes and references

1. E. I. Solomon and S. S. Stahl, *Chem. Rev.*, 2018, **118**, 2299-2301.
2. I. G. Denisov, T. M. Makris, S. G. Sligar and I. Schlichting, *Chem. Rev.*, 2005, **105**, 2253-2278.
3. C. Jung, in *The Ubiquitous Roles of Cytochrome P450 Proteins*, John Wiley & Sons, Ltd, 2007, DOI: 10.1002/9780470028155.ch7, pp. 187-234.
4. T. L. Poulos, *Chem. Rev.*, 2014, **114**, 3919-3962.
5. M. Imai, H. Shimada, Y. Watanabe, Y. Matsushima-Hibiya, R. Makino, H. Koga, T. Horiuchi and Y. Ishimura, *Proc Natl Acad Sci U S A*, 1989, **86**, 7823-7827.
6. W. Zhang, W. Lai and R. Cao, *Chem. Rev.*, 2017, **117**, 3717-3797.
7. M. L. Pegis, C. F. Wise, D. J. Martin and J. M. Mayer, *Chem. Rev.*, 2018, **118**, 2340−2391.
8. S. Dey, B. Mondal, S. Chatterjee, A. Rana, S. Amanullah and A. Dey, *Nat. Rev. Chem.*, 2017, **1**, 0098.
9. C. W. Machan, *ACS Catal.*, 2020, **10**, 2640-2655.
10. G. Passard, A. M. Ullman, C. N. Brodsky and D. G. Nocera, *J. Am. Chem. Soc.*, 2016, **138**, 2925-2928.
11. Y.-H. Wang, P. E. Schneider, Z. K. Goldsmith, B. Mondal, S. Hammes-Schiffer and S. S. Stahl, *ACS Cent. Sci.*, 2019, **5**, 1024-1034.
12. J. P. Collman, R. Boulatov, C. J. Sunderland and L. Fu, *Chem. Rev.*, 2004, **104**, 561-588.
13. J. Rosenthal and D. G. Nocera, *Acc. Chem. Res.*, 2007, **40**, 543-553.
14. R. McGuire Jr, D. K. Dogutan, T. S. Teets, J. Suntivich, Y. Shao-Horn and D. G. Nocera, *Chem. Sci.*, 2010, **1**, 411.
15. D. K. Dogutan, S. A. Stoian, R. McGuire, M. Schwalbe, T. S. Teets and D. G. Nocera, *J. Am. Chem. Soc.*, 2011, **133**, 131-140.
16. B. D. Matson, C. T. Carver, A. Von Ruden, J. Y. Yang, S. Raugei and J. M. Mayer, *Chem. Commun.*, 2012, **48**, 11100-11102.
17. C. T. Carver, B. D. Matson and J. M. Mayer, *J. Am. Chem. Soc.*, 2012, **134**, 5444-5447.
18. S. Chatterjee, K. Sengupta, B. Mondal, S. Dey and A. Dey, *Acc. Chem. Res.*, 2017, **50**, 1744-1753.
19. S. Bhunia, A. Rana, P. Roy, D. J. Martin, M. L. Pegis, B. Roy and A. Dey, *J. Am. Chem. Soc.*, 2018, **140**, 9444-9457.
20. A. Singha, K. Mittra and A. Dey, *Dalton Trans.*, 2019, **48**, 7179-7186.
21. A. C. Brezny, S. I. Johnson, S. Raugei and J. M. Mayer, *J. Am. Chem. Soc.*, 2020, **142**, 4108-4113.
22. (a) M. L. Pegis, D. J. Martin, C. F. Wise, A. C. Brezny, S. I. Johnson, L. E. Johnson, N. Kumar, S. Raugei and J. M. Mayer, *J. Am. Chem. Soc.*, 2019, **141**, 8315-8326. (b) M. L. Pegis, B. A. McKeown, N. Kumar, K. Lang, D. J. Wasylenko, X. P. Zhang, S. Raugei, J. M. Mayer, *ACS Cent. Sci.* 2016, **2**, 850-856.
23. *See Supporting Information for details.*
24. For solubility of dioxygen in DMF with 0.1 M electrolyte, see: H. J. James and R. F. Broman, *Anal. Chim. Acta*, 1969, **48**, 411-417.
25. D.-H. Chin, G. N. La Mar and A. L. Balch, *J. Am. Chem. Soc.*, 1980, **102**, 4344-4350.